Sensors & Diagnostics

PAPER

View Article Online
View Journal

Cite this: DOI: 10.1039/d6sd00063k

Bacteria-on-chip: a multiplexed point-of-care electrochemical platform for rapid detection of *Escherichia coli* and antimicrobial susceptibility testing

Sonal Fande,[ab] Areon Banerjee[c] and Sanket Goel *[ac]

Urinary tract infections (UTIs), primarily caused by *Escherichia coli* (*E. coli*), are among the most prevalent bacterial infections, affecting millions of individuals each year. Along with this, the rising prevalence of antibiotic resistance poses a major clinical challenge, underscoring the need for rapid and accurate pathogen identification and antimicrobial susceptibility testing (AST). However, conventional diagnostic methods are often costly, labour-intensive, and associated with long turnaround times. To address these limitations, this study presents a fully portable, smartphone-integrated, multiplexed electrochemical platform for the selective detection of *E. coli* DH5α and rapid AST. An indium tin oxide (ITO)-based three-electrode system functionalized with gold nanoparticles was used for sensitive detection of *E. coli* DH5α. The immunosensor was fabricated by immobilizing monoclonal antibodies (mAbs) specific to *E. coli* DH5α onto the functionalized gold surface. The platform achieved a limit of detection of 1.67×10^7 CFU mL^{-1}, with a detection range from 2.76×10^7 to 3.0×10^{10} CFU mL^{-1}. Notably, the detection time is 30 minutes, and the system allows simultaneous testing of four antibiotics within five hours, a substantial improvement over the 2–5 days required by standard AST methods. Furthermore, integrating microfluidic reservoirs with an on-chip heating module enables controlled bacterial incubation and real-time electrochemical detection. This compact handheld platform offers a rapid, sensitive, and multiplexed diagnostic solution to combat antimicrobial resistance.

Received 25th March 2026,
Accepted 14th May 2026

DOI: 10.1039/d6sd00063k

rsc.li/sensors

1. Introduction

Rapid and cost-effective detection of microbial infections at the point of care (POC) remains a critical need in modern healthcare,[1] particularly as commensal bacteria such as *Escherichia coli* (*E. coli*) increasingly evolve into multidrug-resistant pathogens. *E. coli*, a Gram-negative bacterium, is ubiquitous in humans, animals, and environmental reservoirs and is associated with a wide range of infections, including diarrhea, bacteremia, and, most notably, urinary tract infections (UTIs).[2,3] UTIs are the most widespread bacterial infections, affecting nearly 150 million people annually.[4–6] These infections arise from the colonization of microorganisms within the urinary tract and exhibit a higher incidence in females, primarily due to the anatomical predisposition.[7,8] A significant proportion of UTIs are initiated by Gram-negative bacteria, with *E. coli*.[9] In general, UTIs are clinically diagnosed when the microbial concentration in urine reaches or exceeds 10^5 colony-forming units (CFU) mL^{-1}.

Antibiotics are the standard treatment for UTIs; however, their widespread and often indiscriminate use has significantly accelerated the emergence of antimicrobial resistance (AMR), rendering many first-line therapies ineffective. This results in prolonged infections, severe complications, and an increased risk of acute kidney infections or kidney failure.[10,11] The emergence of AMR is driven by the selective pressure exerted by antibiotics, which promotes genetic mutations and the development of resistant bacterial strains. This highlights the importance of understanding the effects of antibiotics and their efficacy against pathogens. Antibiotic susceptibility testing (AST) is critical in combating AMR and ensuring effective treatment.[12,13] AST identifies the causative pathogen, selects the effective antibiotic therapy, and determines the minimum inhibitory concentration (MIC).[14]

[a] *MEMS, Microfluidics and Nanoelectronics (MMNE) Lab, Birla Institute of Technology and Science (BITS) Pilani, Hyderabad Campus, Hyderabad 500078, India. E-mail: sgoel@hyderabad.bits-pilani.ac.in*
[b] *Department of Pharmacy, Birla Institute of Technology and Science (BITS) Pilani, Hyderabad Campus, Hyderabad 500078, India*
[c] *Department of Electrical and Electronics Engineering, Birla Institute of Technology and Science (BITS) Pilani, Hyderabad Campus, Hyderabad 500078, India*

Despite advancements in AST techniques, several challenges, such as long turnaround times (4–5 days), poor sensitivity at low bacterial loads, labour-intensive protocols, and limited accuracy and automation, hinder timely and precise diagnosis.[15–17] Traditional diagnostic methods, including dipstick urinalysis, Gram staining, and routine culture, are commonly used to detect UTIs and AST. While these methods are crucial, they have certain limitations. Furthermore, the dipstick is a prevalent diagnostic tool that effectively detects bacterial growth above 10^5 CFU mL^{-1} but reduces sensitivity for lower bacterial concentrations.[18,19] Routine culturing methods, such as the disk diffusion technique, are regarded as the gold standard due to their capability to assess multiple antibiotics simultaneously.[19,20] However, they do not provide MIC values, essential for accurate treatment regimens. Similarly, Gram staining is a simple and accessible technique, but it requires considerable reagent volumes and tends to have higher margins of error. Moreover, commonly used methods in clinical laboratories, such as spectroscopic, colorimetric, turbidimetric, and cytometric techniques, aim to streamline procedures but are mostly expensive and infrastructure-dependent, limiting their utility in POC. These limitations significantly delay treatment, as this technique typically takes 4 to 5 days; such delays can increase infections and, in severe cases, may lead to fatal effects. Therefore, there is a critical need for rapid diagnostic tests (RDTs) that can quickly identify the causative microorganisms and their corresponding resistance profiles.[21,22]

Recent advances have sought to overcome these limitations. For instance, Pan *et al.* developed a self-assembled monolayer-coated electrochemical biosensor for detecting lactoferrin in UTIs. This developed sensor achieved a LoD of 145 pg mL^{-1} with minimal sample preparation, indicating its potential for rapid diagnostics.[18] However, the sensor is limited to lactoferrin detection and does not offer pathogen-specific identification. Further, Li *et al.* developed a handheld centrifugal force-based handyfuge microfluidic chip, or handyfuge-AST, for on-site AST.[23] It enables rapid determination of MICs for various antibiotics against *E. coli* in 5 hours using a simple handheld centrifugation method. However, the device has primarily been validated only for single testing, limiting its applicability to a broader range of clinically significant pathogens.[23] Similarly, Kang *et al.* have developed a CRISPR/Cas12a-based compact biosensor integrated with loop-mediated isothermal amplification (LAMP) to detect antibiotic resistance genes in water samples. This biosensor demonstrates impressive sensitivity, detecting concentrations as low as 2.75×10^3 copies per mL using both fluorescence and lateral flow assays. However, the developed methods face challenges for large-scale and on-site monitoring due to complex sample processing and high costs.[24] The development of rapid, sensitive, miniaturized, and portable diagnostic technologies holds significant potential to address the limitations of current methods. This could transform clinical management of bacterial infections by enabling timely, targeted therapy, ultimately reducing global morbidity and mortality. Therefore, it is critical to address these challenges and facilitate early disease detection, and maintain the efficacy of existing antibiotics.[25]

To address these challenges, this study presents a fully portable, smartphone-enabled diagnostic device for detecting pathogens and their corresponding antibiotic resistance profiles. The device incorporates advanced features, including a gold nanoparticle (AuNPs)-enhanced multiplexed electrochemical immunosensor, a closed-loop temperature control system, a microfluidic reservoir, and a printed heater, enabling streamlined workflows for bacterial culturing, detection, and AST within a single platform. The system is designed to simultaneously analyze four samples within five hours, significantly improving diagnostic throughput. A key feature of the device is a modular sensing architecture: the electrochemical sensor module is swappable *via* a user-friendly quick-swipe mechanism and securely interfaces with a multichannel electrochemical potentiostat circuitry. The device is powered by a compact battery that feeds a voltage regulator and a temperature controller, maintaining an incubation temperature of 37 °C and built-in thermal cut-off mechanisms. The device operates on electrochemical principles comprising working (W), reference (R), and counter (C) electrodes (E). The WE surface is functionalized with AuNPs to enhance surface area and electron transfer kinetics, followed by immobilization of anti-*E. coli* DH5α monoclonal antibodies (mAb). When bacterial cells or antibiotic-treated samples interact with specific antigens, antibody interactions occur, resulting in measurable electrochemical signals.

The developed biosensing platform demonstrated a wide dynamic range from 2.76×10^7 to 3.0×10^{10} CFU mL^{-1}, with a limit of detection (LoD) $\sim 1.67 \times 10^7$ CFU mL^{-1}. The obtained LoD falls within the clinically relevant bacterial load range observed in UTIs, where significant bacteriuria is typically defined as $>10^6$ CFU mL^{-1}. Specificity assays confirmed selective testing of *E. coli*, with an RSD of 2.5%. Furthermore, batch-to-batch reproducibility studies revealed sensor variability of less than 5%. The device can detect bacteria within 30 minutes and perform AST within 5 hours. Importantly, the entire device is fabricated using cost-effective, rapid-prototyping techniques, making it a highly accessible and scalable solution for real-time, decentralized, and POC microbial diagnostics that meets the urgent global need for rapid, sensitive, and multiplexed AMR screening. While the current sensitivity is suitable for detecting moderate to severe infections, further improvements will be required for early-stage detection with lower bacterial counts.

2. Experimental section

2.1 Materials

Luria–Bertani (LB) broth and agar used for bacterial culture preparation were obtained from Sigma-Aldrich, USA. A glass

slide (50 mm × 50 mm) coated with indium tin oxide (ITO) was obtained from Shilpa Enterprises, Mumbai, India. Potassium chloride, ammonium phosphate, sodium sulfate, sodium phosphate monobasic monohydrate ($NaH_2PO_4{\cdot}H_2O$), ammonium diphosphate, sodium phosphate dibasic dihydrate ($Na_2HPO_4{\cdot}2H_2O$), magnesium chloride, calcium chloride, creatinine, bovine serum albumin (BSA), and urea were obtained from Sigma-Aldrich, USA. *E. coli* culture was obtained from the Department of Biological Sciences at the Birla Institute of Technology and Science, Pilani, Hyderabad campus. An anti-*E. coli* monoclonal antibody was purchased from Thermo Fisher Scientific, USA. Cephalexin, ceftriaxone, sulfamethoxazole, and nitrofurantoin, used for the AST studies, were purchased from Sigma-Aldrich. Polydimethoxysilane (PDMS) was acquired from Delta Silicon, Mumbai, India. CO_2 laser (VLS 3.20) procured from Universal Laser Systems, AZ, USA. Isopropyl alcohol (IPA), polyvinyl chloride (PVC) sheets, and 96-well plates were purchased from Sigma Aldrich, USA. AY321 UV exposure unit was procured from Silicon Ark Electronics, Cambridgeshire, UK. SU-8 dry film photoresist (DFR) was procured from Dupont Electronic Technologies, NC, USA, and the CUTE Vacuum Plasma System from Femto Science, South Korea. Gold nanoparticles (AuNPs) and Anteobind were sourced from Sigma-Aldrich.

All experiments were performed in accordance with the Guidelines of the Medical Centre at BITS Pilani, Hyderabad Campus and approved by the Medical Officer of the Medical Centre at BITS Pilani, Hyderabad Campus. Informed consents were obtained from human participants of this study.

2.2 Methodology

2.2.1 Fabrication of multiplexed electrode pattern. A multiplexed electrode pattern was fabricated on an ITO-coated glass substrate, integrating four sets of three-electrode systems on a single chip. The electrode design was meticulously created in AutoCAD, ensuring optimal geometric parameters for enhanced electrochemical performance. The finalized design was converted into a DXF format for seamless compatibility with a CO_2 laser system.

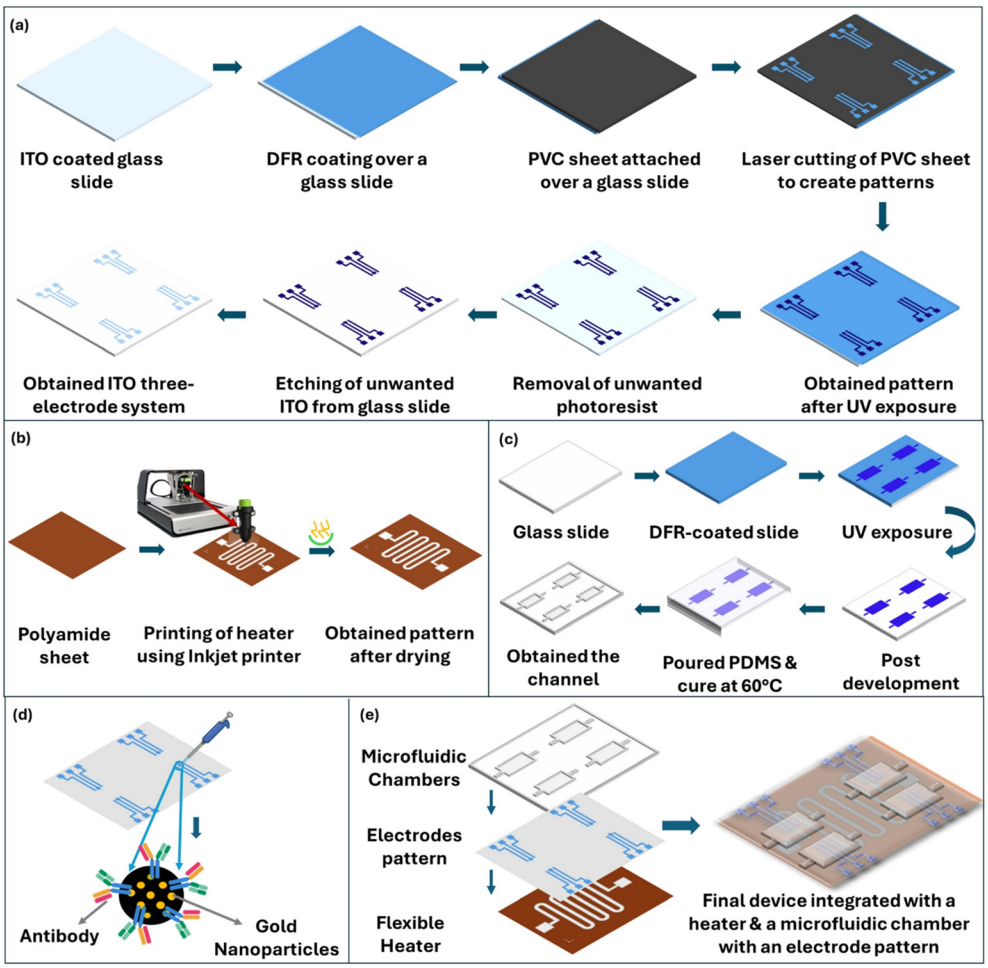

Fig. 1 (a) Stepwise fabrication of an ITO three-electrode system, (b) steps for flexible silver heater fabrication, (c) schematic illustration depicting fabrication process for microfluidic chamber, (d) development of an immunosensor, (e) integrated chip including electrochemical sensor, flexible heater, and microfluidic reservoir.

Fabrication began by thoroughly cleaning the ITO-coated glass substrate (50 mm × 50 mm) with IPA for 15 minutes to remove surface contaminants. Two layers of SU-8 DFR were laminated onto the substrate, achieving a uniform thickness of 70 μm. A PVC sheet was precisely cut using a CO_2 laser to create a mask, operating at 6% power and 10% speed. The prepared mask was then carefully transferred onto the SU-8-coated substrate, followed by UV exposure for 2 minutes to initiate photopolymerization. Subsequently, the mask was removed, and the unexposed SU-8 regions were selectively developed using a 1% sodium carbonate solution. The unexposed ITO regions were then etched using a 1 : 1 hydrochloric acid (HCl) and ferric chloride solution, effectively defining the electrode structures. The final photoresist pattern was removed by immersion in acetone, revealing the final three-electrode pattern (Fig. 1a). The resulting electrode arrays were thoroughly rinsed with IPA to ensure a clean surface. Finally, one electrode was modified with Ag/AgCl ink to serve as a reference electrode.

2.2.2 Fabrication of printed heater. A flexible, inkjet-printed silver microheater was designed to optimize thermal efficiency and enhance mechanical flexibility for bacterial incubation (Fig. 1b). The detailed procedure for fabricating a silver heater on a polyimide (PI) sheet is described in a previous publication by Fande *et al.*[26] Similarly, the serpentine design is printed on the printed circuit board (PCB) using copper traces to achieve uniform heat distribution, and it is integrated into the final, fully automated device.

2.2.3 Designing a microfluidic channel. The requisite microfluidic channel design was prepared in CAD software and patterned onto the glass slide using a photolithographic process similar to that described in section 2.2.1. In brief, a glass substrate having a dimension (75 mm × 50 mm) was coated with DFR 6 times to obtain a suitable microchannel height (35 μm each). The microfluidic channel was patterned using UV exposure and subsequently developed by immersing it in a Na_2CO_3 solution to remove the unwanted photoresist. The microfluidic chip was prepared by pouring PDMS and curing agent (10 : 1) onto the pattern and curing at 70 °C for 1 hour. A PDMS stamped with a microchannel pattern was peeled off the glass substrate. Additionally, a 14-gauge indented hole was punched in the PDMS stamp for the outlet and inlet. The fabrication flow for microfluidic devices is illustrated in Fig. 1c.

2.2.4 Fabrication of an immunosensor for the detection of *E. coli*. AuNPs were carefully drop-casted onto pre-cleaned ITO patterned electrodes to enhance surface area and facilitate efficient antibody immobilization (Fig. 1d). After drying, a 1 : 10 dilution of AnteoBind™ activation reagent was applied on the AuNP-modified surface to promote covalent attachment of the antibodies. The electrodes were then incubated at room temperature to activate the surfaces. Following this, a 100 μg mL^{-1} anti-*E. coli* DH5α mAb was immobilized on the activated surface and incubated at 4 °C for 1 hour to ensure optimal antibody binding. The electrodes were subsequently treated with 1% BSA, a blocking agent that prevents nonspecific adsorption. The resulting immunosensors were utilized for the selective detection of *E. coli* DH5α bacteria.

2.2.5 Integration of electrochemical sensor with microfluidic reservoir and flexible heater. The fabricated electrochemical sensor was seamlessly integrated with microfluidic reservoirs using a two-step process. First, the surfaces were treated with oxygen plasma for 2 minutes to activate them and promote interfacial bonding. Plasma treatment ensured a durable adhesion between the sensor and the microfluidic reservoirs. Following this, the reservoirs were carefully aligned with the electrochemical sensor and thermally cured for 30 minutes to solidify the bond. A printed flexible heater was affixed to the backside of the electrochemical sensor using adhesive tape to incorporate heating functionality. This configuration enabled precise temperature control, creating an optimal environment for bacterial incubation and electrochemical sensing. The integration of these components resulted in a compact, efficient system tailored for on-chip diagnostics. Fig. 1e illustrates the final integrated device for detecting antibiotic-resistant bacteria.

2.2.6 Design and integration of components in a 3D-printed casing. A compact, portable device was developed to enable bacterial incubation, detection, and AST within a fully integrated platform. The system features a bacteria-on-chip setup for culturing bacteria and monitoring their real-time responses to antibiotics. The device features a swappable mechanism, enabling the electrochemical sensor to be easily replaced within a custom-designed, 3D-printed casing. The electrochemical sensor was functionalized by modifying the electrode with AuNPs and then immobilizing anti-*E. coli* antibodies at 4 °C. No thermal treatment was applied during or after the biofunctionalization process. A flexible heater beneath the electrochemical sensor ensures precise thermal control, maintaining an incubation temperature of 37 °C, which is critical for bacterial growth and metabolic activity. A battery powers this heating system through a buck-boost converter, which supplies 1.5 V to the heater. A temperature controller continuously regulates and monitors the heating process for consistency. The heat generated by the flexible heater was efficiently transferred to the bacteria-on-chip, facilitating bacterial incubation. Fabricated electrodes on the chip were connected to a potentiostat *via* a card-edge connector, enabling simultaneous electrochemical monitoring of bacterial activity and antibiotic susceptibility. The entire system was powered by a battery for portability, with an on/off push button for user-friendly operation. All components, including the battery, voltage regulator, temperature controller, and electrochemical sensor, are securely enclosed within a durable 3D-printed casing measuring 100 × 100 × 20 mm^3 ($L \times B \times H$), fabricated *via* layer-by-layer fused deposition modeling. Its compact, modular design, efficient power management, and user-friendly features

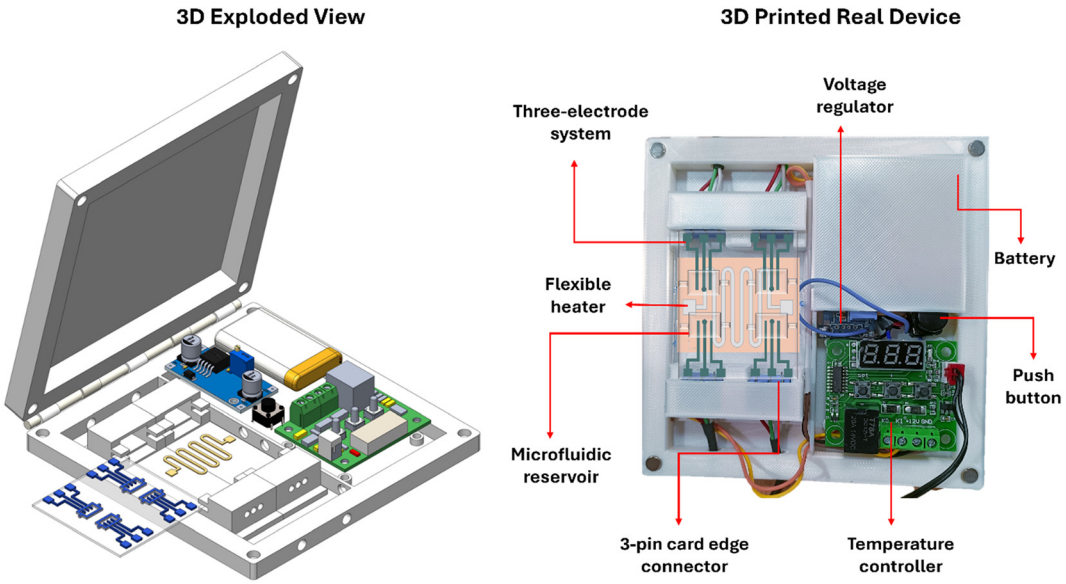

Fig. 2 In-house fabricated 3D-printed compact bacteria-on-chip mini-platform: left side depicts a 3D view diagram, whereas the right side shows a real photograph of the fabricated platform for detecting bacteria and antimicrobial resistance.

make it ideal for POC applications. The 3D illustration and the actual printed device are shown in Fig. 2.

2.2.7 Development of a fully automated portable electrochemical platform. A fully automated and portable electrochemical platform has been developed to enable precise control and analysis of electrochemical reactions, which is crucial for decentralized biomarker detection in POC diagnostics (Fig. 3). The system is built around the ESP32-WROOM-32 model microcontroller, which serves as the central processing unit for efficient signal generation, acquisition, and wireless communication through Bluetooth or Wi-Fi, enabling real-time data transmission for remote diagnostics and monitoring. The potentiostat circuitry integrates a digital-to-analog converter (DAC) and an analog-to-digital converter (ADC) to accurately generate and measure electrochemical signals, supporting advanced electrochemical techniques such as cyclic voltammetry (CV), differential pulse voltammetry (DPV), and electrochemical impedance spectroscopy (EIS). The design also incorporates voltage step-down converters to ensure stable, low-noise power regulation, enabling reliable operation in battery-powered portable devices. All electronic components, including the potentiostat circuitry, heater, and battery, are assembled on a single compact PCB housed within an ergonomic enclosure. The developed device incorporates a printed heater for precise temperature control and incubation, a capacitive touchscreen display for visualizing electrochemical signals and readout, and a rechargeable power supply unit that powers both the potentiostat PCB. A specially designed tray sensor mechanism ensures precise electrical and physical contact between the biosensor strip and the potentiostat interface, enabling accurate electrochemical measurements across the electrode surface. The outer enclosure features a rectangular power switch for easy operation and an integrated charging port, ensuring full portability. The entire system is designed with consideration for ergonomic factors and medical device safety requirements. A graphical user interface (GUI) has also been developed to automate potentiostat operations, control measurement parameters, and display real-time signal readouts. The full circuit diagram for the developed potentiostat is included in the SI.

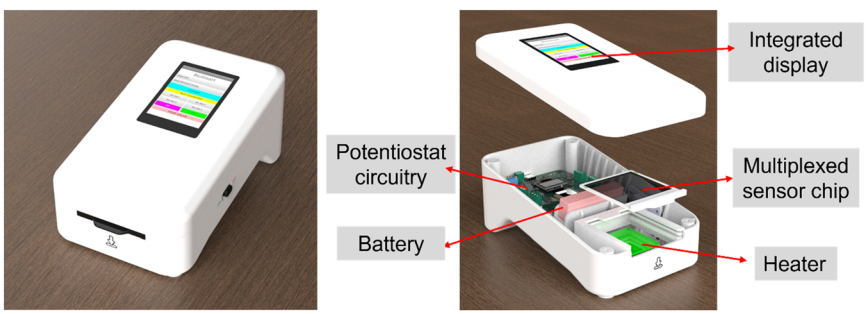

Fig. 3 Developed a fully automated, portable electrochemical platform.

2.2.8 Development of a graphical user interface (GUI). The Android-based application was developed using the MIT App Inventor development kit to enable seamless control of the developed potentiostat circuitry. The developed GUI enables configuration of experimental parameters, selection of specific potentiostat channels, initiation of electrochemical measurements, and real-time visualization of data. The GUI communicates with the potentiostat through Bluetooth Low Energy (BLE), and selected parameters are transmitted to the ESP32, which dynamically generates waveforms and timing configurations for the electrochemical measurement. Real-time data visualization is enabled by a live plotting module that continuously updates incoming data, enabling real-time monitoring of electrochemical reactions using CV, DPV, and EIS (Fig. 4).

2.2.9 Bacterial sample preparation. Prior to experimentation, the bacterial culture was inoculated into LB broth and incubated overnight to promote optimal growth (OD ~1.0). The cultured bacterial solution was then transferred into a sterile tube and centrifuged at 2500 rpm for 5 minutes to pellet the bacterial cells. The pellet was resuspended in 0.1 M PBS (pH 7.4) to maintain physiological conditions. Serial dilutions were performed to achieve a final dilution of 10^9. From each dilution, 10 μL was plated onto agar and incubated at 37 °C for 12 hours. Colony counts were performed on plates containing 30–300 colonies (Fig. 5). The colony-forming unit (CFU) values were used to calculate the bacterial concentration (CFU mL^{-1}) for a quantitative assessment of the bacterial colonies present in the sample.

2.2.10 Off-Chip MIC calculation. The MIC for selected antibiotics, including nitrofurantoin, cotrimoxazole, ciprofloxacin, and fosfomycin, were determined by broth microdilution. A 1 mg mL^{-1} stock solution was prepared for each antibiotic. Working dilutions were subsequently prepared for each antibiotic according to the CLSI guideline.[27–29] The final concentrations used for MIC calculation were nitrofurantoin 2–512 μg mL^{-1}, fosfomycin 8–512 μg mL^{-1}, cotrimoxazole 1.19/0.0625–76/4 μg mL^{-1}, and ciprofloxacin 0.0625–4 μg mL^{-1}. A two-fold serial dilution was performed in a 96-well microplate. The first well served as a negative control, containing only sterile broth medium, while the second well contained the broth medium inoculated with the bacterial culture (growth control). The antibiotic working solution was mixed with the bacterial suspension, and broth medium was added to the third well. Serial dilutions were carried out from the third well onward to the tenth well to create an antibiotic concentration gradient. The well plate was then incubated overnight at 37 °C. Bacterial growth was quantitatively assessed through visual observation after incubation, and the MIC was determined by observing the minimal concentration of the antibiotics at which no visible bacterial growth occurred.

2.2.11 Electrochemical measurement of the sensor. The electrochemical performance of the fabricated device was evaluated by cyclic voltammetry (CV) at 50 mV s^{-1} and differential pulse voltammetry (DPV) with a pulse amplitude of 50 mV, a pulse width of 60 ms, a pulse period of 50 ms, and a step potential of 4 mV. A redox probe solution comprising 1 μM methylene blue in 0.1 M PBS was drop-cast

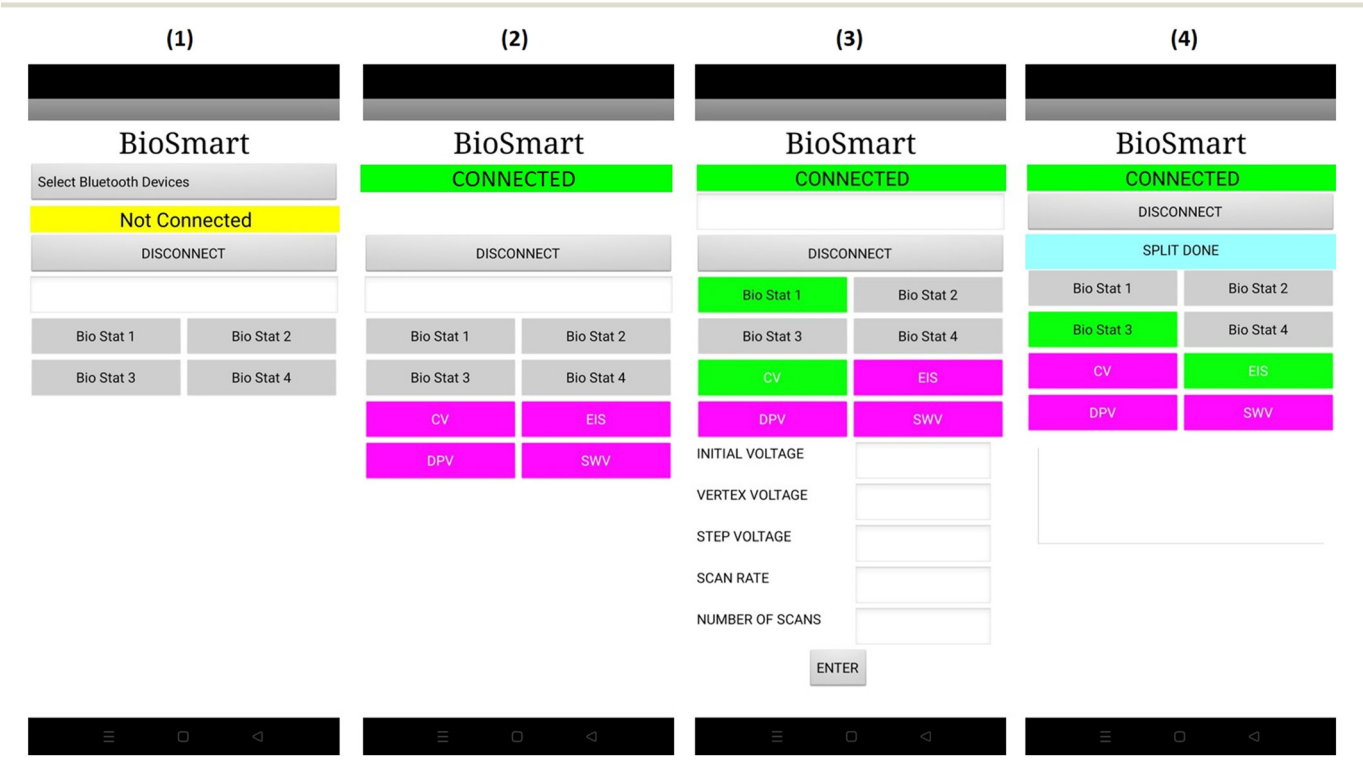

Fig. 4 Image of the developed graphical user interface (GUI) for electrochemical measurements: (1) home page, (2) Bluetooth connection page, (3) analysis page for entering input parameters, and (4) results page displaying the electrochemical measurement data.

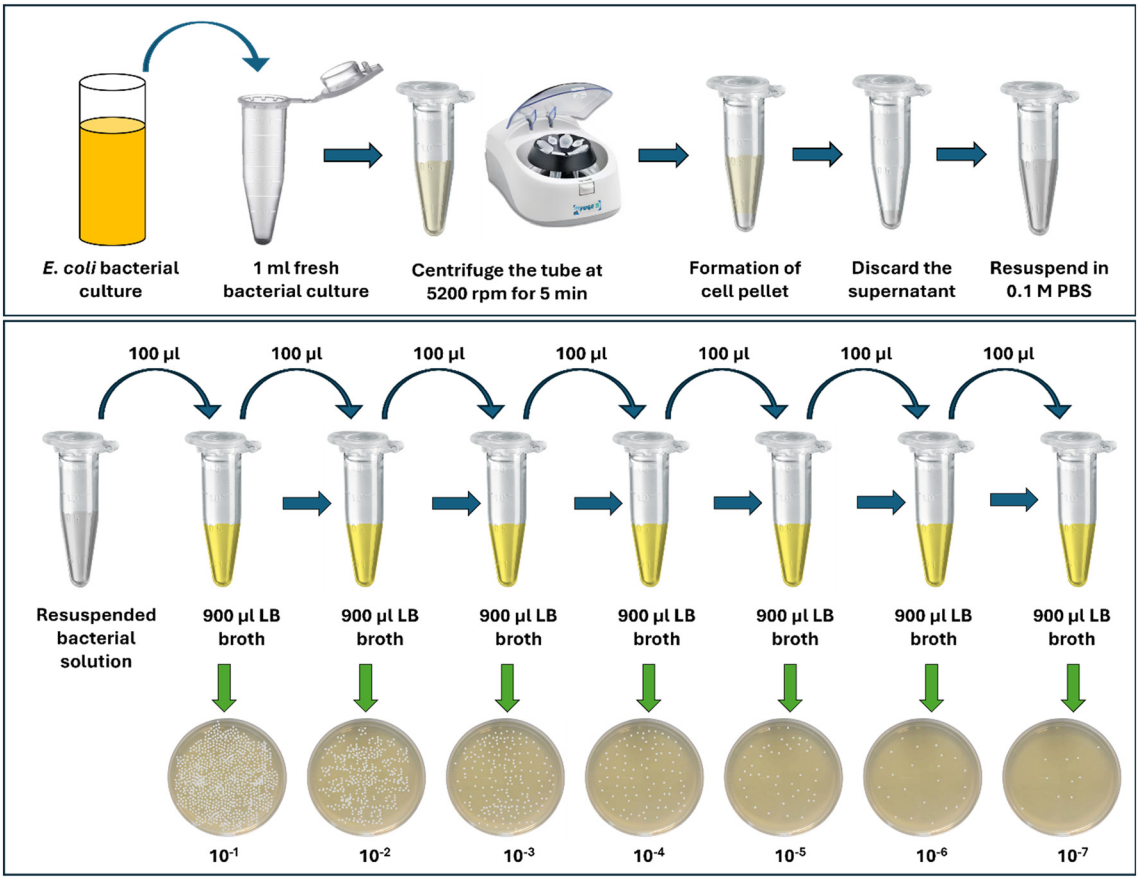

Fig. 5 The stepwise procedure for preparation of different concentrations of the bacteria using the serial dilution method and CFU mL^{-1} calculation from each incubated plate.

onto the WE surface. For antimicrobial resistance testing, a mixture of the antibiotic solution and the bacterial suspension was introduced into the device's microfluidic chamber. Electrochemical measurements were conducted to monitor changes in peak signals resulting from interactions between the pathogen and the antibody and antibiotics.

3. Results and discussion

3.1 Off-chip MIC calculation

The MICs of four selected antibiotics, such as nitrofurantoin, cotrimoxazole, ciprofloxacin, and fosfomycin, were determined using *E. coli* (DH5α strain) as a model microorganism. The distinct MIC values are summarised in Table 1, revealing varying degrees of antibacterial efficacy against *E. coli*. These results provide a reference baseline for evaluating the effectiveness of antibiotics in subsequent on-chip electrochemical assays.[30,31]

Table 1 MIC values for various antibiotics against *E. coli* DH5α

Sr. no	Antibiotics	Concentration (µg mL^{-1})	MIC (µg mL^{-1})
1	Nitrofurantoin	2–512	32
2	Cotrimoxazole	1.19/0.0625–76/4	2/32
3	Ciprofloxacin	0.0625–4	0.25
4	Fosfomycin	8–512	64

3.2 Morphological characterization

Field-emission scanning electron microscopy (FESEM) was employed to study the surface morphology of the fabricated electrode. Fig. 6 displays FESEM micrographs of a bare electrode and a functionalized electrode with gold nanoparticles (AuNPs). In Fig. 6a, the bare electrode appears to have a smooth, uniform surface with minimal topographical features, indicating a clean substrate prior to modification. In contrast, Fig. 6b reveals a uniformly distributed pattern of bright, spherical nanostructures corresponding to the deposited AuNPs. These nanoparticles exhibit minimal aggregation and are well-dispersed across the electrode surface. The change in surface texture and density of the nanostructures confirms the successful coating of AuNPs on the electrode, thereby increasing the effective surface area and introducing electrochemically active sites.

3.3 Electrochemical characterization

The electrochemical characterization of the developed immunosensor was investigated using CV to evaluate surface modification and functionalization. The sensor was modified

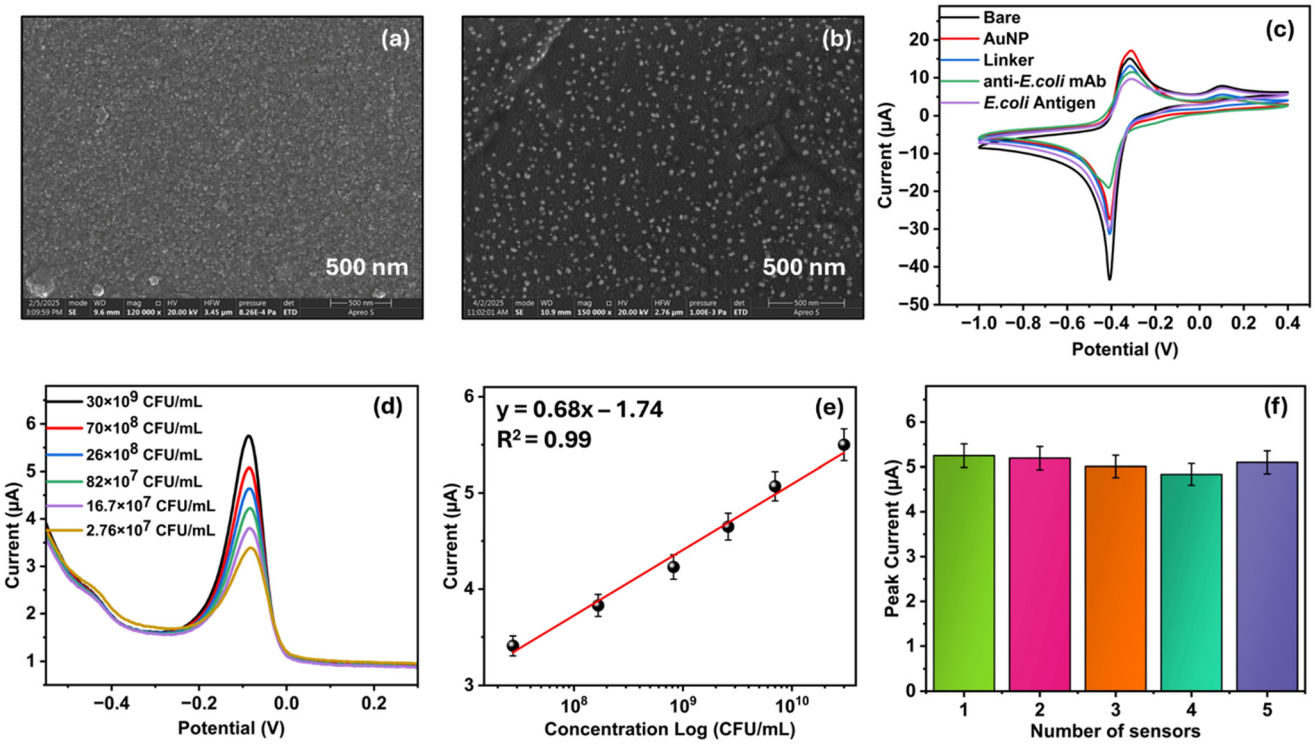

Fig. 6 Morphological study using FE-SEM of the electrode surface: (a) bare electrode, and (b) electrode modified with AuNPs; electrochemical performance of the developed immunosensor: (c) layer-by-layer electrochemical characterization demonstrates changes in CV response at each modification step of the sensor surface, (d) DPV responses were recorded for varying concentrations of *E. coli* DH5α, ranging from 2.76 × 10^7 to 3.0 × 10^{10} CFU mL^{-1}, (e) calibration curve showing a linear correlation between peak current and the logarithm of *E. coli* concentration, (f) reproducibility study using five independently fabricated sensors (n = 3).

in a stepwise manner, and CV was recorded after each modification. As shown in Fig. 6c, the peak current decreases progressively with each successive modification step, indicating successful surface modification due to increased interfacial resistance resulting from biomolecule immobilization. The immobilization of anti-*E. coli* mAb onto the AuNP-modified electrode surface resulted in a further decline in current, confirming effective antibody attachment. Subsequent incubation with *E. coli* DH5α antigen led to additional signal suppression, attributed to the formation of antigen–antibody complexes, thereby validating the selective biorecognition capability of the biosensor.

3.4 On-chip electrochemical detection of bacteria

Fig. 6d illustrates the DPV responses of the developed immunosensor across a concentration range of 2.76 × 10^7 to 3.0 × 10^{10} CFU mL^{-1} of *E. coli* DH5α. A progressive decrease in peak current was observed as bacterial concentration increased, attributed to the formation of antigen–antibody complexes at the sensor interface. This biorecognition event forms an insulation layer on the sensor surface, thereby hindering electron transfer and ion diffusion at the electrode–electrolyte interface and, consequently, reducing the electrochemical signal. The corresponding calibration curve (Fig. 6e), which plots the logarithm of bacterial concentration against peak current, exhibits a well-defined inverse correlation. The developed immunosensor demonstrates LoD and LoQ values of 1.67 × 10^7 CFU mL^{-1} and 1.49 × 10^8 CFU mL^{-1}, respectively, indicating its potential for quantitative microbial diagnostics.

3.5 Performance optimization of the immunosensor

The reproducibility of the sensor was evaluated by fabricating five independent electrodes under identical conditions within a single batch. As illustrated in Fig. 6f, the peak current responses showed minimal variation across devices, indicating consistent sensor performance. The calculated RSD was 3%, confirming reproducibility and reliability of the immunosensor fabrication process.

The specificity of the developed immunosensor was evaluated against non-target bacterial species, including *E. coli* K12, *Pseudomonas aeruginosa* (*P. A*), *Staphylococcus aureus* (*S. A*), and *Streptococcus pneumoniae* (*S. P*), and the results are represented in Fig. 7a. The immunosensor was incubated with a microbial cocktail comprising *E. coli* DH5α (10^5 CFU mL^{-1}) mixed with *E. coli* K12, *P. A*, *S. A*, and *S. P* (each at 10^5 CFU mL^{-1}). As illustrated in Fig. 7a, the peak current response remained consistent with that observed for the target pathogen alone, demonstrating that the sensor

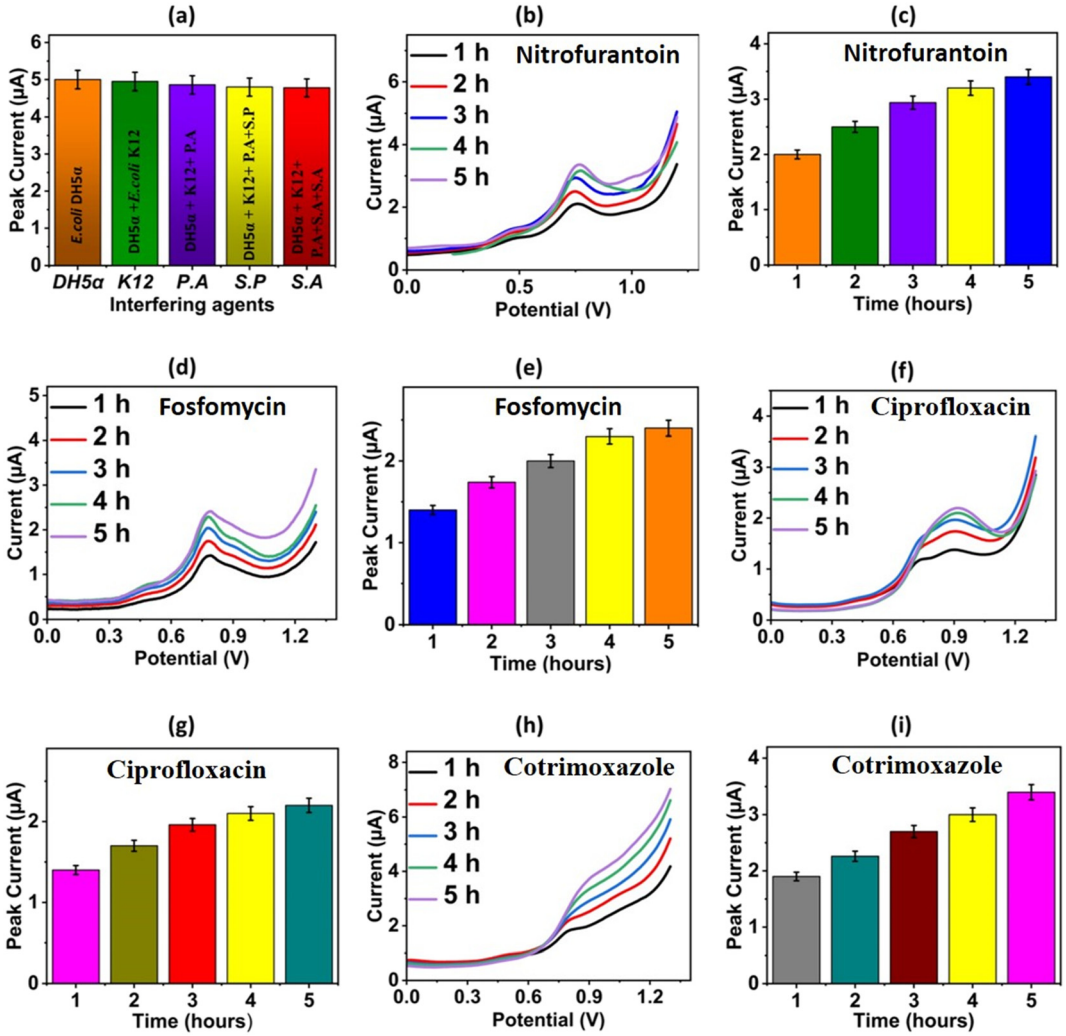

Fig. 7 (a) Bar graph illustrating the specificity performance of the developed immunosensor containing mixed bacterial suspension for all strains, (b) a DPV graph of nitrofurantoin at 32 μg mL^{-1}, (c) corresponding histogram for nitrofurantoin showing time dependent inhibition, (d) a DPV graph of the fosfomycin at 64 μg mL^{-1}, (e) corresponding histogram for fosfomycin, (f) a DPV graph of ciprofloxacin at 0.25 μg mL^{-1}, (g) corresponding histogram for the ciprofloxacin, (h) a DPV graph of the cotrimoxazole at 2/32 μg mL^{-1}, (i) corresponding histogram for the cotrimoxazole.

retained its specificity even in the presence of other bacterial species. These results confirm the selective response of the developed immunosensor toward *E. coli* DH5α, with negligible competitive binding from co-existing microorganisms. The % RSD across the non-target species was 2.5%, indicating minimal signal variation and negligible interference.

3.6 Detection of *E. coli* in the urine sample

The analytical performance of the developed immunosensor was further evaluated using artificial urine spiked with known concentrations of *E. coli* DH5α to simulate real clinical conditions. The immunosensor demonstrated detection capability, with recovery rates ranging from 96% to

Table 2 Detection of *E. coli* DH5α from the artificial urine sample using the developed Au/anti-*E. coli* mAb/*E. coli* immunosensor

Sample	Added CFU mL^{-1}	Peak current (μA)	Found CFU mL^{-1}	Recovery (%)
Artificial urine	4.00×10^9	5.78	3.91×10^9	99.75%
	7.90×10^8	5.15	7.98×10^8	101%
	1.44×10^8	4.48	1.47×10^8	102%
	2.90×10^7	3.83	2.86×10^7	98.62%
Human urine	4.00×10^9	5.8	4.11×10^9	103%
	7.90×10^8	5.13	7.6×10^8	96.20%
	1.44×10^8	4.45	1.37×10^8	95.14%
	2.90×10^7	3.85	3.0×10^7	104%

101% (Table 2), indicating high accuracy and minimal matrix interference. These results further confirm the potential of the immunosensor for robust, reliable detection of *E. coli* in complex biological fluids. Further, the performance of the immunosensor was evaluated in a real human urine sample. The urine samples were collected from a healthy volunteer in accordance with the ethical guidelines. Morning urine samples obtained after 8 hours of fasting were preferred due to their reliability. Samples were collected in sterilized, packaged bottles. The collected urine was tested electrochemically by diluting the sample 1 : 20 and spiking it with different concentrations of the *E. coli* DH5α pathogen. Table 2. Showed the recovery of 95.14 to 103%, showing its reliability in a real human sample.

3.7 Electrochemical detection of AST

The antimicrobial activity of four clinically relevant antibiotics, including nitrofurantoin, fosfomycin, ciprofloxacin, and a combination of sulfamethoxazole/trimethoprim (cotrimoxazole), against *E. coli* was studied using a developed immunosensor. All the measurements were performed in triplicate (n = 3). Fig. 7b–i shows the time-dependent response to antibiotics. In the presence of antibiotics, the observed increase in peak current is attributed to changes at the electrode–electrolyte interface associated with bacterial metabolic activity. In the absence of effective antibiotics, viable bacteria tend to form a surface-associated layer that hinders electron transfer, resulting in a lower current response. In contrast, in the presence of effective antibiotics, bacterial growth is inhibited, resulting in reduced surface coverage and reduced impedance to electron transfer, thereby increasing the measured peak current.[28] Fig. 7b and c show the response of nitrofurantoin (32 μg mL^{-1}) to bacterial growth, demonstrating a linear increase in peak current with incubation time, which indicates inhibition of bacterial activity. Beyond 4 hours, the change in peak current was minimal, indicating complete inhibition between 3 and 4 hours. Similarly, fosfomycin (Fig. 7d and e) exhibits bacteriostatic activity, with a rise in current over time. Fig. 7f and g show the DPV response and histogram for ciprofloxacin (0.25 μg mL^{-1}), with a sharp increase in current over 2 hours and minimal changes thereafter. This indicates that ciprofloxacin exhibits rapid inhibitory action, with most bacterial inhibition occurring within 2–3 hours. For cotrimoxazole (Fig. 7h and i), a gradual increase in current response was observed over the 5-hour incubation, indicating continuous inhibition of bacterial growth at the MIC concentration. Table 3 highlights distinct electrochemical inhibition kinetics for each antibiotic, enabling rapid differentiation of antibiotic efficacy against *E. coli*.

3.8 Performance validation of a developed portable potentiostat system

The performance of the developed portable potentiostat was evaluated by interfacing it with both a smartphone and a laptop to assess its functionality under wireless conditions. A 1 mM MB solution in 0.1 M PBS was employed as a redox probe for proof of concept. CV was used to monitor the anodic and cathodic currents as the potential was first scanned in a positive direction and then returned to the negative direction. Fig. 8 presents the CV results for two different electrodes. Fig. 8a illustrates the performance of the ITO electrode, while Fig. 8b and c depict the CV and DPV response of the thin-film-deposited gold electrodes on flexible PI substrates, recorded using a portable battery-powered potentiostat. The CV clearly shows distinct anodic and cathodic peaks corresponding to the reversible redox behavior of MB on both electrode types. The presence of well-defined redox peaks confirms that the portable device can generate controlled potential sweeps and accurately capture faradaic current responses. Fig. 8d shows the Nyquist plot for a thin-film deposited gold electrode.

Finally, the analytical performance of the developed platform was compared with that of the existing biosensor. Table 4 presents a comparative analysis of the developed electrochemical biosensors for different pathogen detection. While many reported sensors are highly sensitive and deliver results within 15 minutes, most are designed for single-pathogen detection and do not support multiplexing or AST; they are solely focused on detection and lack portability. In contrast, the device developed in this study detects pathogens, supports multiplexing, and performs AST studies. Furthermore, it achieves a detection time of 30 minutes and performs AST within 5 hours, which is comparable to other techniques. The combination of non-invasive sample compatibility, analytical performance, and portability gives this device a distinct advantage over existing technologies. The relatively higher detection limit observed in this study is due to the primary focus on the proof-of-concept. Further sensitivity improvements are anticipated by optimizing the sensing interface, which includes utilizing advanced nanomaterials of varying sizes and ratios.

Table 3 Electrochemical AST results for different antibiotics against *E. coli*

Antibiotic	MIC conc	Electrochemical response	Inhibition time
Nitrofurantoin	32 μg mL^{-1}	Peak current increases to 4 h, then stabilizes	Complete inhibition at 3–4 h
Fosfomycin	64 μg mL^{-1}	Gradual increase in current throughout 5 h	Slow, progressive inhibition
Ciprofloxacin	0.25 μg mL^{-1}	Sharp rise in current within the first 2 h, then minimal change	Rapid inhibition within 2–3 h
Cotrimoxazole	2/32 μg mL^{-1}	Continuous increase in current over 5 h	Continuous inhibition over 5 h

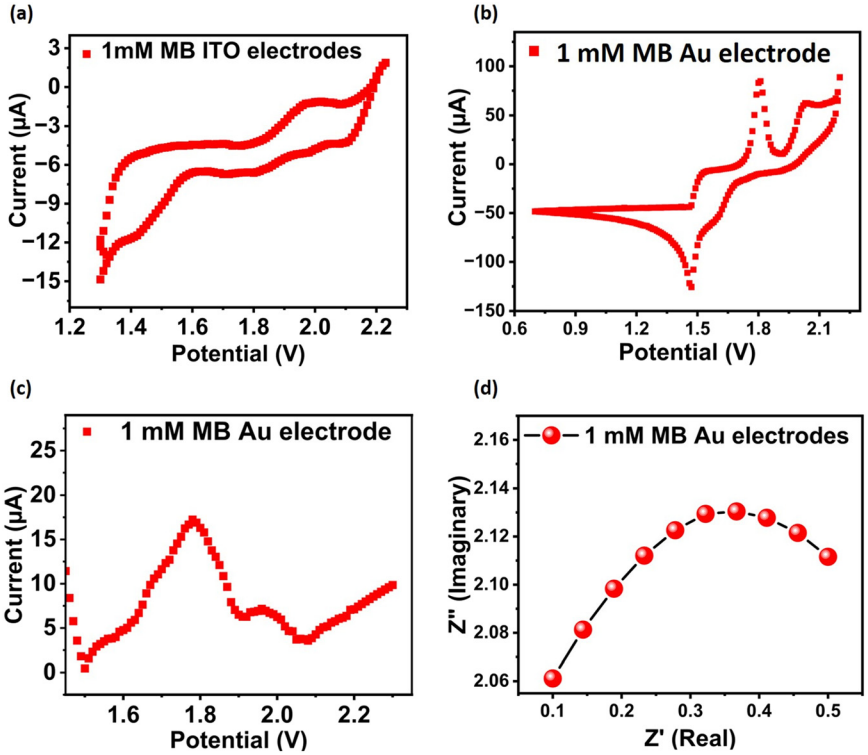

Fig. 8 Voltammetric profile of 1 mM MB in 0.1 M PBS recorded using the developed portable potentiostat at a scan rate of 50 mV: (a) CV study for ITO electrode; (b) CV study for gold electrodes; (c) DPV study for gold electrodes (pulse amplitude = 50 mV s^{-1}, pulse width = 50 ms, step potential = 4 mV); (d) EIS study for gold electrodes (recorded in 1 mM MB over the frequency range of 1 kHz to 100 mHz with AC amplitude of 10 mV).

Table 4 Comparison of the developed pathogen detection platform with existing electrochemical biosensors

Target pathogen	Detection limit	Multi-plexing	Detection time	AST	Portability	Sample matrix	Ref.
Strep. Pneumoniae	4.50 pM	No	15 min	No	Lab-based	Serum	1
Salmonella	1.12×10^2 CFU mL^{-1}	No	40 min	No	Lab based	Milk	32
E. coli	11.8 CFU mL^{-1}	No	30 min	No	Lab based	Milk and pork	33
Stap. aureus	1.23×10^2 CFU mL^{-1}	No	25 min	No	Lab based	Blood plasma	34
E. coli	34 CFU mL^{-1}	No	15 min	No	Lab based	Water, urine, and milk	35
L. monocytogene	2.6 CFU mL^{-1}	No	1.5 h	No	Lab based	Fruits	36
E. coli	10 CFU mL^{-1}	No	1 h	No	Lab based	Juice, milk, and serum	37
E. coli	1.67×10^7 CFU mL^{-1}	Yes	30 min	Yes	Portable	Urine	This work

(Strep = Streptococcus, Stap = Staphylococcus, E. = Escherichia, L. = listeria)

4. Conclusion

This study presents a portable, fully automated device capable of detecting bacterial pathogens and their antibiotic resistance profiles within five hours. The system integrates an on-chip heating module, temperature controller, power source, and a miniaturized electrochemical sensor into a compact, custom-designed casing. Coupled with a microfluidic chamber, the platform enables efficient sample handling while maintaining optimal conditions for bacterial incubation and electrochemical analysis. The device employs a three-electrode configuration comprising an AuNP-modified indium tin oxide (ITO) working electrode functionalized with anti-*E. coli* DH5α monoclonal antibodies for the selective detection of *E. coli* DH5α, an Ag/AgCl-modified reference electrode, and an ITO counter electrode. The platform demonstrated good reproducibility, with a relative standard deviation (RSD) of approximately 3.0%, and achieved a sensitivity of 0.684 μA $\log(\text{CFU mL}^{-1})^{-1}$. Furthermore, the device offers multiplexing, enabling simultaneous testing of four antibiotics. Overall, this portable platform represents a scalable point-of-care solution for rapid antimicrobial resistance profiling, with significant potential for deployment in both clinical and field settings. Future studies will aim to enhance sensitivity for lower detection limits. Additionally, the platform will be validated with a larger number of clinical samples and a broader range of antibiotics to fully establish its clinical applicability. The proposed platform has potential

for integration into broader clinical health systems for decentralized antimicrobial resistance monitoring and rapid point-of-care diagnostics. Future improvements could incorporate advanced sensing strategies, such as photoelectrochemical detection, to enable continuous, dynamic monitoring of bacterial growth and antibiotic response by facilitating more accurate MIC determination.[38] In addition, using advanced nanomaterials, including graphene-based structures and emerging two-dimensional materials such as phosphorene and related systems, may further enhance sensitivity and signal performance.[39–41] These approaches offer promising avenues for improving the platform's analytical capabilities and clinical applicability.

Author contributions

Sonal Fande: conceptualization, data curation, formal analysis, writing – original draft, validation, investigation. Areon Banerjee: methodology, formal analysis, software. Sanket Goel: conceptualization, supervision, project administration, writing – review & editing, validation, funding acquisition.

Conflicts of interest

The authors declare that they don't have no known competing interests or personal relationships that could have appeared to influence the work reported in this paper.

Data availability

The data supporting this article have been included in the main article and/or as part of the supplementary information (SI).

Supplementary information: includes the potentiostat circuit diagram and a demonstration video of the developed system. See DOI: https://doi.org/10.1039/d6sd00063k.

Acknowledgements

The work was funded by the Indian Council of Medical Research (ICMR) under the ICMR Senior Research Fellowship (ICMR-SRF) scheme (Grant No. 5/3/8/45/ITR-F/2022). The author would like to thank the Central Analytical Laboratory (CAL) facilities, BITS Pilani, Hyderabad Campus, for providing access to characterization equipment. The author would also like to thank Shashwat Goel for his guidance on GUI development.

References

1 V. Vezza, V. Mani, N. Docherty, A. Butterworth, D. Alcorn, P. A. Hoskisson and D. Corrigan, *Sens. Diagn.*, 2026, **5**, 596–610, DOI: 10.1039/d5sd00210a.
2 N. Naidoo and O. T. Zishiri, Presence, Pathogenicity, Antibiotic Resistance, and Virulence Factors of Escherichia coli: A Review, *Bacteria*, 2025, **4**, 16, DOI: 10.3390/bacteria4010016.
3 N. Baskaran, R. Sakthivel, C. S. Karthik, Y. C. Lin, X. Liu, H. W. Wen, W. Yang and R. J. Chung, *Talanta*, 2025, **282**, 127008, DOI: 10.1016/j.talanta.2024.127008.
4 E. K. Sher, A. Džidić-Krivić, A. Sesar, E. K. Farhat, A. Čeliković, M. Beća-Zećo, E. Pinjic and F. Sher, *Pharmacol. Ther.*, 2024, **261**, 108688, DOI: 10.1016/j.pharmthera.2024.108688.
5 Z. Zhang, G. Ogata, K. Asai, T. Yamamoto and Y. Einaga, *ACS Sens.*, 2023, **8**, 4245–4252, DOI: 10.1021/acssensors.3c01569.
6 A. Capstick, F. Palermo, K. Zakka, N. Fletcher-Lloyd, C. Walsh, T. Cui, S. Kouchaki, R. Jackson, M. Tran, M. Crone, K. Jensen, P. Freemont, R. Vaidyanathan, M. Kolanko, J. True, S. Daniels, D. Wingfield, R. Nilforooshan and P. Barnaghi, *NPJ Digit. Med.*, 2024, **7**(1), 11, DOI: 10.1038/s41746-023-00995-5.
7 E. K. Sher, A. Džidić-Krivić, A. Sesar, E. K. Farhat, A. Čeliković, M. Beća-Zećo, E. Pinjic and F. Sher, *Pharmacol. Ther.*, 2024, **261**, 108688, DOI: 10.1016/j.pharmthera.2024.108688.
8 E. K. Sher, A. Džidić-Krivić, A. Sesar, E. K. Farhat, A. Čeliković, M. Beća-Zećo, E. Pinjic and F. Sher, *Pharmacol. Ther.*, 2024, **261**, 108688, DOI: 10.1016/j.pharmthera.2024.108688.
9 J. Chen, X. Liu, J. Tang, K. Fang, J. Jiang, C. Gu, T. Jiang and K. Wu, *Biosens. Bioelectron.*, 2025, **269**, 116948, DOI: 10.1016/j.bios.2024.116948.
10 J. Chen, X. Liu, J. Tang, K. Fang, J. Jiang, C. Gu, T. Jiang and K. Wu, *Biosens. Bioelectron.*, 2025, **269**, 116948, DOI: 10.1016/j.bios.2024.116948.
11 A. Capstick, F. Palermo, K. Zakka, N. Fletcher-Lloyd, C. Walsh, T. Cui, S. Kouchaki, R. Jackson, M. Tran, M. Crone, K. Jensen, P. Freemont, R. Vaidyanathan, M. Kolanko, J. True, S. Daniels, D. Wingfield, R. Nilforooshan and P. Barnaghi, *NPJ Digit. Med.*, 2024, **7**(1), 11, DOI: 10.1038/s41746-023-00995-5.
12 E. Wenzler, M. Maximos, T. E. Asempa, L. Biehle, A. N. Schuetz and E. B. Hirsch, *Pharmacotherapy*, 2023, **43**, 264–278, DOI: 10.1002/phar.2781.
13 S. Al-Madhagi, S. Elwary, L. F. Abuqatouseh and M. Zourob, *Sens. Diagn.*, 2026, **5**, 404–412, DOI: 10.1039/d5sd00130g.
14 M. A. Salam, M. Y. Al-Amin, J. S. Pawar, N. Akhter and I. B. Lucy, *Saudi J. Biol. Sci.*, 2023, **30**(3), 103582, DOI: 10.1016/j.sjbs.2023.103582.
15 R. Purbowati, S. L. Utami, D. Raharjo and M. Masfufatun, *J. Multidiscip. Appl. Nat. Sci.*, 2025, **5**(1), 1–9, DOI: 10.47352/jmans.2774-3047.222.
16 S. Fande, K. Amreen, D. Sriram, V. Mateev and S. Goel, *Sensors*, 2023, **23**(23), 9314, DOI: 10.3390/s23239314.
17 D. Han, X. Li, X. Bian, J. Wang, L. Kong, S. Ding and Y. Yan, *Sens. Actuators, B*, 2022, **355**, 131120, DOI: 10.1016/j.snb.2021.131120.
18 Y. Pan, G. A. Sonn, M. L. Y. Sin, K. E. Mach, M. C. Shih, V. Gau, P. K. Wong and J. C. Liao, *Biosens. Bioelectron.*, 2010, **26**, 649–654.
19 B. Crane, J. P. Hughes, S. J. Rowley Neale, M. Rashid, P. E. Linton, C. E. Banks and K. J. Shaw, *Analyst*, 2021, **146**, 5574–5583, DOI: 10.1039/D1AN00850A.

20 S. Srikanth, U. S. Jayapiriya, S. K. Dubey, A. Javed and S. Goel, *iScience*, 2022, **25**(11), 105388, DOI: 10.1016/j.isci.2022.105388.
21 M. Fritzenwanker, M. O. Grabitz, V. Negwer, O. Schwengers, B. Arneth, T. Chakraborty, C. Imirzalioglu and F. Wagenlehner, *Eur. J. Clin. Microbiol. Infect. Dis.*, 2025, **44**(3), 703–715, DOI: 10.1007/s10096-024-05030-3.
22 C. Celik Yoldas, N. Temur, N. Ildiz, P. Sagiroglu, M. A. Atalay, A. Yilmaz, E. Gokturk and I. Ocsoy, *Analyst*, 2026, **151**(6), 1669–1678, DOI: 10.1039/d5an01356a.
23 S. Li, C. Wan, B. Wang, D. Chen, W. Zeng, X. Hong, L. Li, Z. Pang, W. Du, X. Feng, P. Chen, Y. Li and B. F. Liu, *Anal. Chem.*, 2023, **95**, 6145–6155, DOI: 10.1021/acs.analchem.3c00557.
24 K. Mao, H. Zhang, F. Ran, H. Cao, R. Feng, W. Du, X. Li and Z. Yang, *J. Hazard. Mater.*, 2024, **462**, 132793, DOI: 10.1016/j.jhazmat.2023.132793.
25 C. Wan, A. Qu, M. Li, R. Tang, L. Fu, X. Liu, P. Wang and C. Wu, *Anal. Chem.*, 2022, **94**, 732–739, DOI: 10.1021/acs.analchem.1c03100.
26 S. Fande, K. Amreen, D. Sriram and S. Goel, *IEEE Access*, 2025, **13**, 36590–36600, DOI: 10.1109/ACCESS.2025.3544132.
27 M. Li, C. Zhang, G. Chen, L. Nahar, S. D. Sarker and M. Guo, *J. Pharm. Biomed. Anal.*, 2020, **181**, 113122, DOI: 10.1016/j.jpba.2020.113122.
28 Y. Xu, Y. Jiang, C. Li, Y. Chen and Y. Yang, *J. Electroanal. Chem.*, 2020, **877**, 114534, DOI: 10.1016/j.jelechem.2020.114534.
29 C. Tellapragada, B. Hasan, A. Antonelli, A. Maruri, C. de Vogel, D. Gijón, M. Coppi, A. Verbon, W. van Wamel, G. M. Rossolini, R. Cantón and C. G. Giske, *Clin. Microbiol. Infect.*, 2020, **26**, e1–e7, DOI: 10.1016/j.cmi.2020.01.026.
30 T. Khare, S. Mahalunkar, V. Shriram, S. Gosavi and V. Kumar, *Environ. Res.*, 2021, **199**, 111321, DOI: 10.1016/j.envres.2021.111321.
31 I. O. Chikezie, *Afr. J. Microbiol. Res.*, 2017, **11**(23), 977–980, DOI: 10.5897/AJMR2017.8545.
32 S. Li, Y. Zhang, M. Guo, Z. Yi, M. Hu, C. Xiong, G. Huang and J. Zhang, *Talanta*, 2024, **270**, 125576, DOI: 10.1016/j.talanta.2023.125576.
33 Y. Zhou, Z. Li, J. Huang, Y. Wu, X. Mao, Y. Tan, H. Liu, D. Ma, X. Li and X. Wang, *Bioelectrochemistry*, 2023, **150**, 108345, DOI: 10.1016/j.bioelechem.2022.108345.
34 D. Patel, Y. Zhou and R. P. Ramasamy, *J. Electrochem. Soc.*, 2021, **168**(5), 057523, DOI: 10.1149/1945-7111/abef85.
35 A. H. Dabhade, B. Paramasivan, A. S. Kumawat and B. Saha, *Talanta*, 2025, **285**, 127306, DOI: 10.1016/j.talanta.2024.127306.
36 M. Zhang, Y. Chen, S. G. Liu and X. Shi, *Microchem. J.*, 2023, **194**, 109357, DOI: 10.1016/j.microc.2023.109357.
37 J. Zhang, M. Zhou, L. Yang, B. Huang, K. Lu, H. Wen and J. Ren, *Sens. Actuators, B*, 2025, **422**, 136609, DOI: 10.1016/j.snb.2024.136609.
38 Y. Zhang, Z. Chen, S. Wei, Y. Zhang, H. Fu, H. Zhang, D. Li and Z. Xie, *Exploration*, 2024, **4**(5), 20230128, DOI: 10.1002/EXP.20230128.
39 Z. Xie, C. Xing, W. Huang, T. Fan, Z. Li, J. Zhao, Y. Xiang, Z. Guo, J. Li, Z. Yang, B. Dong, J. Qu, D. Fan and H. Zhang, *Adv. Funct. Mater.*, 2018, **28**(16), 1705833, DOI: 10.1002/adfm.201705833.
40 Z. Xie, Y. Duo, T. Fan, Y. Zhu, S. Feng, C. Li, H. Guo, Y. Ge, S. Ahmed, W. Huang, H. Liu, L. Qi, R. Guo, D. Li, P. N. Prasad and H. Zhang, *Light: Sci. Appl.*, 2022, **11**(1), 324, DOI: 10.1038/s41377-022-00980-9.
41 Z. Xie, M. Peng, R. Lu, X. Meng, W. Liang, Z. Li, M. Qiu, B. Zhang, G. Nie, N. Xie, H. Zhang and P. N. Prasad, *Light: Sci. Appl.*, 2020, **9**(1), 161, DOI: 10.1038/s41377-020-00388-3.